REFERENCES AND NOTES

1. H. Toynbee and T. Mackenzie, *Nature* **33**, 245 (1886); J. D. Everett and W. H. Everett, *ibid.* **68**, 599 (1903).
2. O. H. Vaughan, Jr., and B. Vonnegut, *J. Geophys. Res.* **94**, 13179 (1989).
3. R. J. Nemzek and J. R. Winckler, *Geophys. Res. Lett.* **16**, 1015 (1989).
4. The TV camera, scheduled for flight on the SCEX (Several Coordinated Experiments) sounding rocket experiment, was an ITT model 4562 ICID with a sensitivity of 10E-5 lux and was capable of recording 6.5-magnitude stars in normal real-time operation.
5. R. E. Orville (National Lightning Detection Network), personal communication; W. Lyons (R-Scan), personal communication.
6. C. B. Moore and D. Raymond, personal communication.
7. C. T. R. Wilson, *Proc. R. Soc. London* **236**, 297 (1956).
8. C. V. Boys, *Nature* **118**, 749 (1926).
9. D. J. Malan, *C. R. Acad. Sci.* **205**, 812 (1937).
10. B. Vonnegut, O. H. Vaughan, Jr., M. Brook, *Bull. Am. Meteorol. Soc.* **70**, 1263 (1989).
11. M. A. Uman, *The Lightning Discharge* (Academic Press, San Diego, CA, 1987).
12. B. Vonnegut, C. B. Moore, R. P. Espinola, H. H. Blau, Jr., *J. Atmos. Sci.* **23**, 764 (1966).
13. C. T. R. Wilson, *Proc. R. Soc. London* **37**, 32D (1925).
14. R. A. Helliwell and M. G. Morgan, *Proc. IRE* **47**, 200 (1959).
15. R. A. Helliwell, *Whistlers and Related Ionospheric Phenomena* (Stanford Univ. Press, Stanford, CA, 1965).
16. W. C. Hoffman, *J. Geophys. Res.* **65**, 2047 (1960).
17. M. C. Kelly *et al.*, *ibid.* **90**, 9815 (1985); R. H. Holzworth *et al.*, *ibid.*, p. 9824.
18. U. S. Inan *et al.*, *ibid.* **93**, 11455 (1988).
19. We thank the many colleagues who have provided reference material and relevant data, including C. B. Moore, M. Brook, W. C. Armstrong, R. E. Orville, W. Lyons, and D. Raymond. We also thank P. J. Kellogg, principal investigator of the SCEX rocket experiment, for the chance to test the TV camera. SCEX is supported by National Aeronautics and Space Administration grant NSG 5373 at the University of Minnesota. The Winckler program at Minnesota in Space Plasma Physics is supported by NASA grant NSG 5088.

17 January 1990; accepted 19 April 1990

Seawater Strontium Isotopic Variations from 2.5 Million Years Ago to the Present

R. C. CAPO* AND D. J. DEPAOLO

Measurements of marine carbonate samples indicate that during the past 2.5 million years the $^{87}Sr/^{86}Sr$ ratio of seawater has increased by 14×10^{-5}. The high average rate of increase of $^{87}Sr/^{86}Sr$ indicates that continental weathering rates were exceptionally high. Nonuniformity in the rate of increase suggests that weathering rates fluctuated by as much as ±30 percent of present-day values. Some of the observed shifts in weathering rates are contemporaneous with climatic changes inferred from records of oxygen isotopes and carbonate preservation in deep sea sediments.

THE $^{87}Sr/^{86}Sr$ RATIO OF DISSOLVED oceanic Sr changes slowly on geologic time scales in response to changes in the relative rates of weathering of continental surface and ocean floor rocks. This dependence on weathering rates makes the $^{87}Sr/^{86}Sr$ ratio of ancient seawater a monitor of paleoclimate because weathering is both a function of climate and, as a remover of atmospheric carbon dioxide, a major long-term feedback mechanism in the climate system. We have determined the $^{87}Sr/^{86}Sr$ ratio of oceanic dissolved Sr for the past 2.5 million years from measurements on calcium carbonate sediment obtained primarily from DSDP Site 590 (*1*). This period is one in which changes in the seawater Sr isotope ratio can be compared with other proxy records of paleoclimate and paleoceanography, and thereby a more complete reconstruction of Plio-Pleistocene conditions can be obtained.

Site 590 was drilled in 1300 m of water on Lord Howe Rise in the Tasman Sea (31°S). Use of hydraulic piston-coring methods minimized disturbance of the core (*1*). The recovered sediment is pelagic carbonate ooze; it provides a nearly continuous record of carbonate deposition since 15 million years ago (Ma) and contains well-preserved calcareous microfossil assemblages and little terrigenous material (*1*). Core 590B was sampled at approximately 3-m intervals to a depth of 30 m; this interval corresponds to about 2×10^5 years. We also measured three deeper samples, which extend the record back to 3.6 Ma, as well as several samples from cores 590 and 590A. We assigned ages to the samples on the basis of paleomagnetic reversal stratigraphy (*2*) and their positions within calcareous nannofossil biozones (*3*), using the time scale of Berggren *et al.* (*4*). In addition, two samples from equatorial Pacific piston core V28-238 (*5*) and two from Hawaiian coral terraces (*6*) were measured. Samples of 15 to 100 mg were dissolved (*7*) and analyzed for $^{87}Sr/^{86}Sr$ ratios and concentrations of K, Rb, and Sr (*8*).

The total variation in the $^{87}Sr/^{86}Sr$ ratio of the oceans is less than 2×10^{-4} between 2.5 and 0 Ma (*9*). In order to study the fine structure of this change, standard measurement errors of less than ±0.00001 are needed. To achieve this we used an automated data collection procedure during mass spectrometer runs that minimizes intermeasurement drift, a more intense Sr^+ ion beam to improve counting statistics (*10*), and an appropriate thermal ionization mass dis-

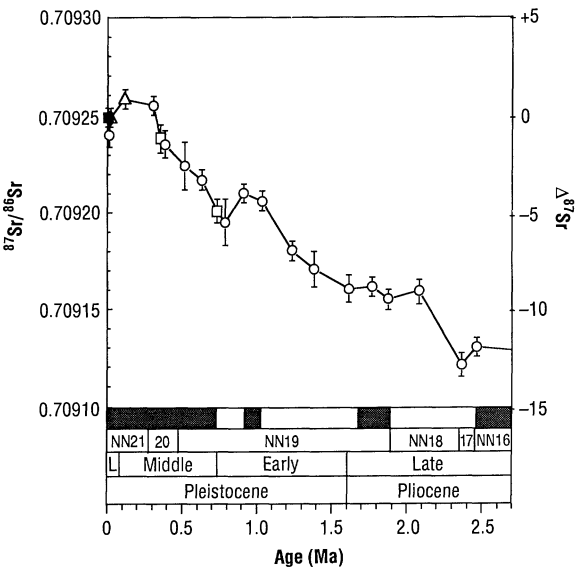

Fig. 1. Measured $^{87}Sr/^{86}Sr$ ratio against age for bulk carbonate ooze from DSDP Site 590 (open circles). Samples were assigned ages based on their positions within calcareous nannofossil stratigraphy (*3*) (lower scale, center) and based on paleomagnetic stratigraphy (*2*) (lower scale, top). The open squares are from core V28-238; the open triangles are from Hawaiian coral terraces. The modern value (solid square) is that for EN-1, the U.S. Geological Survey *Tridacna* Sr isotope standard (0.709249 ± 5); $\Delta^{87}Sr$ is the difference between the measured $^{87}Sr/^{86}Sr$ value and the value for EN-1, multiplied by 10^5. The error limits are ± 2 SEM (Table 1).

R. C. Capo, Berkeley Center for Isotope Geochemistry, Department of Geology and Geophysics, University of California and Earth Science Division, Lawrence Berkeley Laboratory, Berkeley, CA 94720, and Department of Earth and Space Sciences, University of California, Los Angeles, CA 90024.
D. J. DePaolo, Berkeley Center for Isotope Geochemistry, Department of Geology and Geophysics, University of California, and Earth Science Division, Lawrence Berkeley Laboratory, Berkeley, CA 94720.

*To whom correspondence should be addressed.

crimination formulation (*11*). In addition, we closely monitored common sources of artifacts, and performed multiple measurements on each sample (*12*).

The measured $^{87}Sr/^{86}Sr$ ratios (Table 1 and Fig. 1) show that the $^{87}Sr/^{86}Sr$ ratio of the oceans has increased by 14×10^{-5} since 2.4 Ma. This rate of growth (6×10^{-5} per million years) is high in comparison to the average of about 1.5×10^{-5} per million years for the rest of the Pliocene. During the Cenozoic, however, growth rates as high as those observed for the Plio-Pleistocene occurred in five other short periods (~38, 23.5 to 22, 18 to 15.5, 11.5 to 11.0, and 6.2 to 5.5 Ma) (Fig. 2) (*9, 13*).

In detail, the $^{87}Sr/^{86}Sr$ seawater curve for Site 590 (Fig. 1) exhibits an apparent cyclicity with a period of about 0.8 million years. The periods of rapid growth are 2.4 to 2.1, 1.6 to 0.9, and 0.8 to 0.3 Ma. The remaining periods in the last 3 million years have been times of nearly zero growth or of a decreasing $^{87}Sr/^{86}Sr$ ratio; this includes the last 0.3 million years before the present. The most noticeable discontinuity in the data from DSDP 590 samples (0.9 to 0.8 Ma) was confirmed by sample V28-238-1.2, which can be correlated precisely with Site 590 because of the identification of the Brunhes-Matuyama magnetic reversal at 0.73 Ma (*2, 5*).

The rate of change of the $^{87}Sr/^{86}Sr$ ratio of oceanic Sr (R') can be expressed as

$$R' = N_0^{-1} \Sigma J_i (R_i - R) \quad (1)$$

where N_0 is the number of moles of Sr in the oceans, J_i is the flux of Sr to the ocean from the ith source, R_i is the $^{87}Sr/^{86}Sr$ ratio of Sr from the ith source, and R is the $^{87}Sr/^{86}Sr$ ratio of seawater. Defining the mean value of the $^{87}Sr/^{86}Sr$ ratio being added to the ocean as (*14*)

$$R_{in} = \Sigma(J_i R_i)/\Sigma J_i \quad (2)$$

gives

$$R = R_{in} - (N_0/\Sigma J_i)R' \quad (3)$$

To model observed changes in the $^{87}Sr/^{86}Sr$ ratio with time (t) (Fig. 1), we assume that N_0 is constant and use the mean values of R and R' for each segment of the curve in Eq. 1. One of the three J_i or three R_i values is then solved for while the other five parameters are kept constant and equal to the values in Table 2. The derived values of $J_i(t)$ or $R_i(t)$ are then inserted in Eq. 2 to give $R_{in}(t)$.

The rapidity and magnitude of the observed shifts in R' imply that they result from changes in the riverine Sr input rather than changes in the seafloor basalt or sediment alteration fluxes (*15*). Shifts in the hydrothermal alteration flux (J_h) are unlikely to be the cause of the observations because fluctuations in J_h of up to 100% in 10^5 years would be required to produce the observed seawater $^{87}Sr/^{86}Sr$ variations. Dating of marine magnetic anomalies offers no evidence of changes in seafloor spreading rates for this period, which would be the likely cause of variations in the hydrothermal alteration flux (*16*). Similarly, the marine carbonate dissolution and recrystallization flux is unlikely to be the main process responsible. Even the complete cessation of

Table 1. Sample locations, trace element concentrations and Sr isotope data.

Sample*	Depth (m)	Zone†	Age (Ma)	K (ppm)	Sr (ppm)	$^{87}Rb/^{86}Sr$	Measured $^{87}Sr/^{86}Sr$	±‡	Average $^{87}Sr/^{86}Sr$	±
590 1-1	0.2	NN21	0.01				0.709242	9	0.709241	5
							0.709241	7		
							0.709241	9		
							0.709241	10		
HC-170-5			0.014		6463		0.709246	14	0.709250	9
							0.709255	19		
HC-287-6			0.120	128	1864	0.0043	0.709260	20	0.709258	5
							0.709256	23		
590B-1-1	1.0	NN20	0.30	439	1476	0.0010	0.709261	24	0.709255	5
							0.709250	18		
				466	1724	0.0005	0.709254	33		
							0.709255	18		
V28-238-0.6	0.6	NN19	0.35				0.709234	6	0.709238	7
							0.709241	10		
590B-2-1	3.0	NN19	0.38	495	1652	0.0010	0.709238	41	0.709235	7
							0.709228	34		
				543	1646	0.0007	0.709240	11		
590B-2-3	6.0	NN19	0.51	613	1690	0.0016	0.709218	25	0.709224	12
				617	1716	0.0010	0.709230	17		
590B-2-5	9.0	NN19	0.63	530	1238	0.0009	0.709218	14	0.709216	5
							0.709215	12		
V28-238-1.2	1.2	NN19	0.73	304	1510	0.0018	0.709198	15	0.709201	6
							0.709204	18		
590B-3-1	12.6	NN19	0.78	716	1675	0.0017	0.709210	32	0.709195	12
							0.709187	25		
				467	1495	0.0014	0.709185	31		
							0.709199	10		
590B-3-3	15.6	NN19	0.91	723	1643	0.0011	0.709210	13	0.709210	5
(forams)				56	1331	0.0007	0.709210	12		
(forams)				4	357	0.0012	0.709209	17		
590B-3-5	18.6	NN19	1.03	518	1728	0.0009	0.709204	16	0.709206	5
					1638	0.0022	0.709204	30		
							0.709210	9		
590B-4-1	22.2	NN19	1.23	451	2205	0.0006	0.709181	14	0.709180	5
							0.709178	13		
590B-4-3	25.2	NN19	1.38	453	1886	0.0007	0.709158	11	0.709171	9
					1865	0.0009	0.709179	10		
							0.709171	9		
							0.709175	10		
590B-4-6	29.7	NN19	1.61	576	2148	0.0010	0.709162	17	0.709161	7
							0.709166	19		
							0.709154	10		
590B-5-2	33.0	NN19	1.77				0.709164	10	0.709162	5
							0.709160	21		
590A-2-1	0.6	NN18	1.88				0.709156	10	0.709155	5
(forams)							0.709154	9		
(forams)							0.709155	9		
590B-5-6	39.0	NN18	2.08	372	1637	0.0013	0.709156	14	0.709159	6
							0.709162	10		
590B-6-3	44.0	NN17	2.37	439	1912	0.0008	0.709125	17	0.709122	6
							0.709119	30		
590A-3-2	1.4	NN16	2.47				0.709132	11	0.709131	5
							0.709130	13		
590B-8-6	68.0	NN16	3.10	393	1892	0.0006	0.709129	21	0.709126	5
							0.709124	15		
590B-12-6	107.0	NN14/15	3.60		1781		0.709121	16	0.709121	16

*Numbers following 590 (or 590A, 590B) indicate core and section number at Site 590. †Calcareous nannofossil zone (3). ‡The reported uncertainty is ±2 SEM.

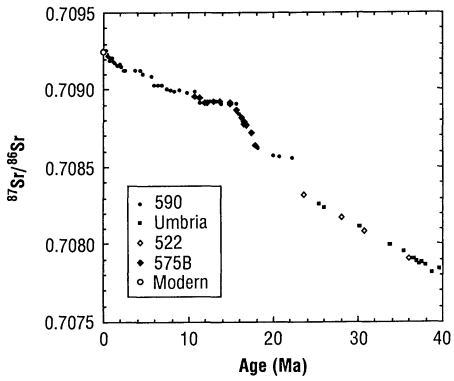

Fig. 2. The $^{87}Sr/^{86}Sr$ evolution of seawater over the past 40 million years based on bulk carbonate isotopic ratios from Sites 590 (solid circles), 522 (open diamonds) and 575B (solid diamonds) corrected for diagenesis [see (7) and Table 1], and measured values for Late Eocene and Oligocene Scaglia Cinerea chalks and marls from the Umbria region, Italy (solid squares) (*13*). The modern value (open circle) is that for EN-1.

Table 2. Modern parameters for the Sr cycle. The mass of Sr in the ocean (*30*), N_0, is assumed to be 1.21×10^{17} mol; the time constant τ ($= N_0/\Sigma J_i$) is 2.70 million years.

Input source	Flux (10^{10} mol Sr/yr)	$^{87}Sr/^{86}Sr$
Rivers (*26, 27*)	3.0	0.711
Submarine alteration (*28*)	1.2	0.705
Diagenesis (*29*)	0.3	0.7085
	$\Sigma J_i = 4.5$	$R_{in} = 0.709$

dissolution of marine carbonates from 2.5 Ma to the present could not generate the observed increase in the seawater $^{87}Sr/^{86}Sr$ ratio, and the flux of Sr from carbonate diagenesis (J_c) would need to increase by more than an order of magnitude to produce the observed decrease in the $^{87}Sr/^{86}Sr$ ratio at 0.8 Ma.

The most plausible explanation for the observed fluctuations over the last 2.5 Ma is change in the terrigenous input of rivers to the oceans, either by a change in the isotopic composition of rivers (R_r), by a change of the dissolved Sr flux (J_r), or by a combination of these. Because it is difficult to assess the relative importance of changes in R_r as opposed to J_r, we illustrate the variations required by considering two models. Figure 3 shows the seawater $^{87}Sr/^{86}Sr$ curve produced by varying only the riverine $^{87}Sr/^{86}Sr$ ratio (Fig. 3A) or only the riverine Sr flux (Fig. 3B). The observed time dependence of the seawater $^{87}Sr/^{86}Sr$ ratio (R_r) requires variations of about ± 0.0005 in the $^{87}Sr/^{86}Sr$ ratio of riverine Sr (Fig. 3A, top), or fluctuations of about $\pm 30\%$ in J_r relative to its modern value (Fig. 3B, top).

The deduced changes in the product J_rR_r represent changes in the global chemical weathering rate, because it is chemical weathering, mainly of the minerals feldspar and calcite, that releases Sr from continental surface rocks into solution in ground waters and eventually to the oceans. The climatic implications of the results therefore depend on the parameters that affect the global rate of chemical weathering. Qualitatively, weathering rates are believed to increase with erosion rate and precipitation (*17*). The total amount of continental weathering is also presumably dependent on the area of the continents above sea level. All three of these are likely to affect the flux of Sr from the continents, J_r, but it is unknown whether they affect the $^{87}Sr/^{86}Sr$ ratio of riverine Sr (R_r). Changes in R_r would require that the average $^{87}Sr/^{86}Sr$ ratio of the rocks exposed to weathering at and near the earth's surface change, and to account for the variations we observe in the oceanic $^{87}Sr/^{86}Sr$ ratio, this change would have to happen during a short time period. Because of the heterogeneity of crustal rocks (and thus the likelihood that rocks with contrasting $^{87}Sr/^{86}Sr$ ratios are distributed approximately randomly over the continents), this possibility seems remote. Therefore, we attribute shifts in J_rR_r mainly to variations in J_r.

It is unlikely that the J_r variations can be explained simply by the changes in the area of continents above sea level with a constant global mean weathering rate per unit continental area. On the basis of the hypsometric curve of the earth, changes in continental area above sea level of $\pm 35\%$ of the present continental area would require variations in sea level of 200 to 300 m (*18*). This variation substantially exceeds the amount of sea level change (~100 m) believed to have

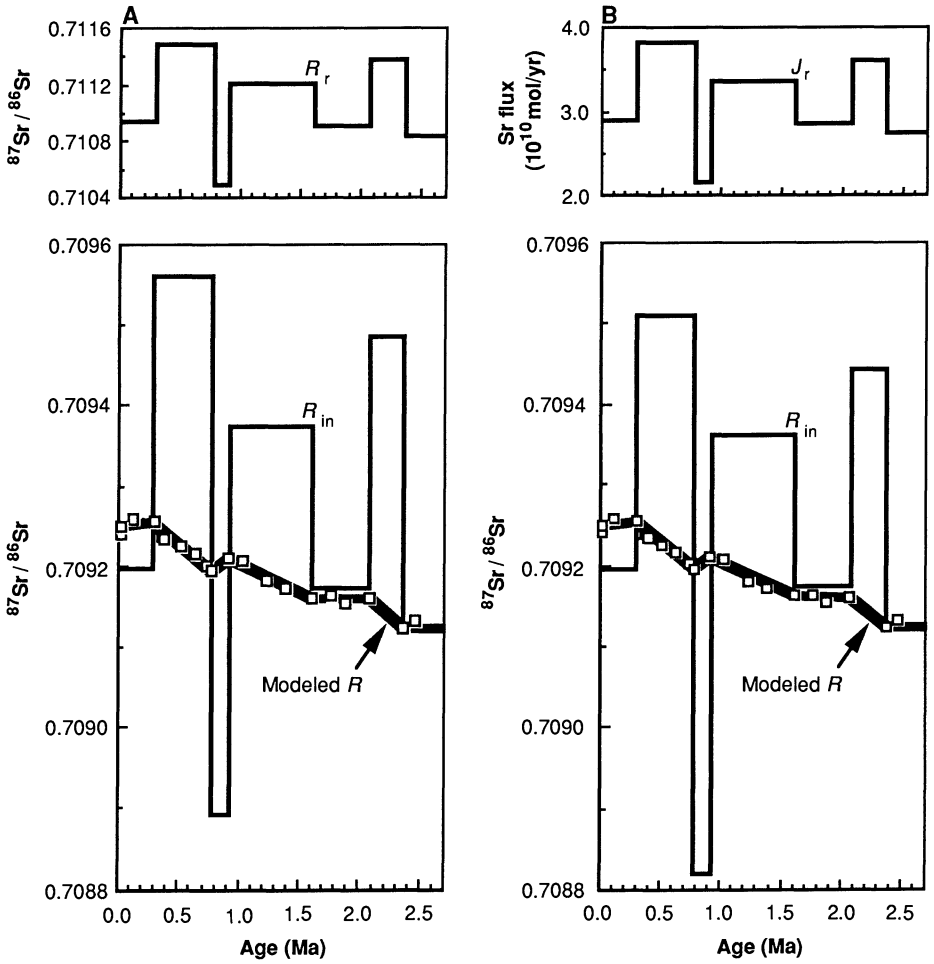

Fig. 3. (**A**) (Top) Variation of the $^{87}Sr/^{86}Sr$ ratio of riverine input (R_r) needed to produce the observed $^{87}Sr/^{86}Sr$ versus age curve of Fig. 1, if all other parameters are kept constant. (Bottom) Model seawater $^{87}Sr/^{86}Sr$ (heavy line) and the average $^{87}Sr/^{86}Sr$ of Sr input to the oceans (R_{in}; light line) corresponding to the R_r curve above. Data from Fig. 1 (open squares) shown for comparison. (**B**) (Top) Values of riverine Sr flux (J_r) necessary to produce the model R curve of (A) (all other parameters are kept constant), and the associated change in R_{in} (light line, bottom).

occurred during the Pleistocene (*19*). Therefore, the data require changes in the mean global rates of erosion or precipitation or both, independent of, or perhaps in conjunction with, changes in mean sea level.

The shift in the J_r curve (Fig. 3B, top) just after 2.4 Ma and the minimum at 0.8 to 0.9 Ma correspond to discontinuities in the oxygen isotope record of foraminifera ($\delta^{18}O$) and to times of exceptionally low carbonate preservation in the deep sea. The discontinuity in $\delta^{18}O$ near 2.4 Ma has been interpreted as the time of onset of major glaciation in the Northern Hemisphere (*20*) and the discontinuity at ~0.8 Ma to a change from high-frequency, low-amplitude climatic oscillations to lower frequency (100 Kyr), higher amplitude oscillations (*21*). The minimum in J_r from 300,000 years ago to the present also corresponds to a period of low $CaCO_3$ preservation (*22*). Poor $CaCO_3$ preservation in the deep sea would be expected for periods of reduced continental erosion and weathering and for periods of high sea level (*23*). The difference in weathering rates inferred from Sr isotopes between 0.8 to 0.3 Ma and 0.3 to 0 Ma is not recognized in other proxy records of paleoclimate.

The apparent period of about 0.8 million years for the variations in the rate of change of oceanic $^{87}Sr/^{86}Sr$ ratio is substantially longer than the main periodicities in the oxygen isotope record and the $CaCO_3$ preservation record. However, this longer period is implicit in discontinuities in these records at 2.4 and 0.8 Ma and in the occurrence of the Pliocene-Pleistocene boundary at 1.6 Ma. Cyclic variations in climatic conditions have been attributed to changes in the pattern of insolation on the earth caused by changes in the earth's orbital parameters (*24*). The longest period of orbital variation predicted from current models is in eccentricity and has a period of about 400,000 years (*25*). If the Sr isotopic variations are related to insolation forcing, either the response is nonlinear or there are additional longer-period insolation cycles.

The difference in mean slope of the $^{87}Sr/^{86}Sr$ curve before and after ~2.4 Ma is a longer time scale feature (Fig. 2). The observation that this change in slope corresponds to the inferred onset of major Northern Hemisphere glaciation suggests that this event caused increased continental weathering. This effect could be understood in terms of rapid cycling between warm and cold global climatic conditions inferred from stable isotope records. The concomitant erosion by continental glaciers interspersed with warm humid periods in the same latitudes might produce exceptionally high mean weathering rates.

REFERENCES AND NOTES

1. J. Kennett *et al.*, *Initial Rep. Deep Sea Drill. Proj.* **90**, 263 (1986).
2. C. Barton and J. Bloemendal, *ibid.*, p. 1273.
3. W. Lohman, *ibid.*, p. 763.
4. W. Berggren, D. Kent, J. Flynn, J. Van Couvering, *Geol. Soc. Am. Bull.* **96**, 1407 (1985).
5. N. Shackleton and N. Opdyke, *Quat. Res.* **3**, 39 (1973).
6. Sample HC170-5 is a coral from a terrace 150 m below sea level with a radiocarbon age of 13,610 ± 50 years ago [J. Moore and D. Fornari, *J. Geol.* **92**, 752 (1984)], and a U-series age of 15.7×10^3 to 15.8×10^3 years ago [B. Szabo and J. Moore, *Geol. Soc. Am. Abstr. Progr.* **20**, 236 (1988)]. Sample HC287-6 is composed of coralline algae from a terrace 360 m below sea level dated at $120 \pm 5 \times 10^3$ years ago [B. Szabo and J. Moore, *Geology* **14**, 967 (1986)].
7. Isotopic ratios were measured in the acetic acid–soluble portions of bulk carbonate samples from Site 590 and core V28-238. Bulk carbonate might be considered more susceptible to post-depositional alteration because the bulk sample has a much smaller average grain size than does a separate of foraminifera tests. However, we found agreement between separated foraminifera and bulk carbonate Sr isotope values (for example, samples 590B-3-3 and 590A-2-1, Table 1). Numerical modeling of diagenesis for Site 590 suggests that there has been no significant post-depositional modification of the $^{87}Sr/^{86}Sr$ ratio of the sediments in the upper 100 m of the Site 590 core [see F. Richter and D. DePaolo, *Earth Planet. Sci. Lett.* **83**, 27 (1987); *ibid.* **90**, 382 (1988)]. Samples were rinsed in an ultrasonic bath with distilled water to remove pore fluid, and then crushed and dissolved in dilute (1.0 molal) acetic acid to avoid contamination with noncarbonate phases [D. DePaolo, F. Kyte, B. Marshall, J. O'Neil, J. Smit, *Earth Planet. Sci. Lett.* **64**, 356 (1983)]. Following evaporation and redissolution in 1.5-N HCl, standard ion-exchange techniques were used to separate Sr for mass spectrometric analysis.
8. Separated Sr was loaded onto single flat Ta filaments in 1.5-N HCl, dried and oxidized in the presence of H_3PO_4. Most samples were analyzed on a VG Isomass 54E single collector mass spectrometer. Peak and background measurements were integrated over a period of 1 s, with a delay of 1.5 s between measurements. Peaks were measured at mass 88, 87, 86, and 84 in sequence; background readings were taken at 1/3 atomic mass units on either side of each peak, also in sequence. Other samples were run on a Sector 54 multi-collector in dynamic mode with 5-s integration times. Concentrations of K, Rb, and Sr were determined by isotope dilution. Maximum total sample blanks for Sr were 100 pg per 1 μg of Sr.
9. D. DePaolo, *Geology* **14**, 103 (1986).
10. A threefold reduction of the SD counting statistics was obtained on many runs by use of a 10^{10}-ohm resistor that allowed measurement of ion beam intensities of up to 4×10^{-10} A. For single collector mass spectrometer analyses, reproducible high precision measurement of the $^{87}Sr/^{86}Sr$ ratio was accomplished by monitoring of the electrometer response time and the ion beam intensity during mass spectrometric runs. We monitored the electrometer response time by measuring a parameter ϵ_τ, which is the difference between the background measured after the $^{88}Sr^+$ peak and that measured before, divided by the intensity of the $^{88}Sr^+$ beam. The background reading at mass 87.7 (measured after the $^{88}Sr^+$ peak) is higher than that at 88.3 because the current in the amplifier from the mass 88 peak does not completely decay away before the background reading is taken. This effect occurs for each isotope peak and therefore approximately cancels in the determination of peak height ratios. However, there is apparently a second, longer time constant to the amplifier response that may be related to the near saturation of the feedback resistor by the large $^{88}Sr^+$ beam and that affects the measurement of the $^{87}Sr^+$ peak. We observed that an increase in ϵ_τ results in a decrease of the measured $^{87}Sr/^{86}Sr$ value. A change of $+1 \times 10^{-4}$ in ϵ_τ results in a lowering of the measured $^{87}Sr/^{86}Sr$ ratio by 3×10^{-5}. If ϵ_τ were unmonitored and varied between measurements it would be a source of additional analytical uncertainty. We monitored ϵ_τ in all mass spectrometer runs and accepted data only when ϵ_τ is within the limits of $2.0 \pm 1.0 \times 10^{-5}$. This technique restricts error from this effect to $<3 \times 10^{-6}$.
11. An exponential law was used to correct for mass discrimination because it describes the observed instrumental mass-dependent fractionation more accurately than linear or power-law equations [W. Russell, D. Papanastassiou, T. Tombrello, *Geochim. Cosmochim. Acta* **42**, 1075 (1978); G. Wasserburg, S. Jacobsen, D. DePaolo, M. McCulloch, T. Wen, *ibid.*, **45**, 2311 (1981)].
12. Another source of artifacts in the data is the nonlinear relation between beam intensity and the resistor voltage amplification; this results in a systematic correlation between beam intensity and $^{87}Sr/^{86}Sr$ ratio. We have calibrated this effect using the NBS987 Sr standard and find that the measured $^{87}Sr/^{86}Sr$ ratio increases by about 1×10^{-5} per volt of $^{88}Sr^+$ beam intensity. To minimize this source of error, samples were measured with an average $^{88}Sr^+$ beam intensity of 4.1 ± 0.1 V, ($4.1 \pm 0.1 \times 10^{-11}$ A $^{88}Sr^+$ or $4.1 \pm 0.1 \times 10^{-10}$ A $^{88}Sr^+$) so that the associated error in the measurement of $^{87}Sr/^{86}Sr$ ratio is $<1 \times 10^{-6}$. The reported values represent at least two separate mass spectrometer analyses of 150 to 400 ratios. The 2 SEM value for the average from a single run is $\pm 1.7 \times 10^{-5}$. From this number it is expected that two or three runs will yield a 2 SEM of 1.2 or 1.0×10^{-5}. Our typical reproducibility is somewhat smaller than this, probably because the SD of the measured ratios from one mass spectrometer run is slightly inflated by effects that are reproducible from run to run. Even samples repeated more than 1 year apart (sample 1-1, for example) give ratios that agree to within ±0.00001. The statistical uncertainty given is 2 SEM. For multiple runs, where N is the number of runs, the error is 2 SEM/$N^{1/2}$. No uncertainty is quoted at less than ±0.000005; Rb/Sr ratios were too low to necessitate any correction to the measured $^{87}Sr/^{86}Sr$ for in situ decay of ^{87}Rb.
13. D. J. DePaolo and B. L. Ingram, *Science* **227**, 938 (1985); R. Capo and D. DePaolo in *The Eocene-Oligocene Boundary in the Marche-Umbria Basin (Italy)*, I. Premoli-Silva, R. Coccioni, A. Montanari, Eds. (*Spec. Pub. I.1*, International Union of the Geological Sciences Subcommittee on Paleogene stratigraphy, Ancona, Italy, 1988), p. 189.
14. The equation defining R_{in} is an approximation; however, for the conditions of our model Eq. 2 is within a few parts per million of the actual value. This error is insignificant in that the true ratios and fluxes of the sources of Sr to the oceans are known only to within a few percent. For a more detailed treatment of these derivations see G. Brass [*Geochim. Cosmochim. Acta* **40**, 721 (1976)] and H. Holland [*The Chemical Evolution of the Atmosphere and Oceans* (Princeton Univ. Press, Princeton, 1984)].
15. D. Hodell, P. Mueller, J. McKenzie, G. Mead, *Earth Planet. Sci. Lett.* **92**, 165 (1989).
16. E. Mankinen and G. Dalrymple, *J. Geophys. Res.* **84**, 615 (1979).
17. R. Stallard, in *Physical and Chemical Weathering in Geochemical Cycles*, A. Lerman and M. Meybeck, Eds. (*NATO ASI Ser. C*, vol. **251**, Kluwer, Dortrecht, 1988); H. Holland, in *The Sea*, C. Emiliani, Ed. (Wiley-Interscience, New York, 1979), p. 763.
18. H. Sverdrup, M. Johnson, R. Fleming, *The Oceans* (Prentice-Hall, Englewood Cliffs, NJ, 1942), p. 19; C. Harrison *et al.*, *Tectonics* **2**, 357 (1983).
19. R. Oldale and C. O'Hara, *Geology* **8**, 102 (1980).
20. N. Shackleton *et al.*, *Nature* **307**, 620 (1984).
21. N. Shackleton and N. Opdyke, *ibid.* **270**, 216 (1977); N. Pisias and T. Moore, *Earth Planet. Sci. Lett.* **52**, 450 (1981); J. Kennett and C. von der Borch, *Initial Rep. Deep Sea Drill. Proj.* **90**, 1493 (1986).
22. J. Farrell and W. Prell, *Paleoceanography* **4**, 447 (1989); Working Group 1, J. Imbrie, chair, *Report of the Second Conference on Scientific Ocean Drilling* (European Science Foundation, Strasbourg, 1987).
23. S. Schlanger, in *Physical and Chemical Weathering in Geochemical Cycles*, A. Lerman and M. Meybeck, Eds. (*NATO ASI Ser. C*, vol. 251, Kluwer, Dortrecht, 1988), p. 323.

24. A. Berger, *Quat. Res.* **9**, 139 (1978); A. Berger, J. Imbrie, J. Hays, G. Kukla, B. Saltzman, Eds., *Milankovitch and Climate: Understanding the Response to Astronomical Forcing* (Reidel, Dortrecht, 1984).
25. J. Imbrie and J. Z. Imbrie, *Science* **207**, 943 (1980); J. Imbrie, *J. Geol. Soc. London* **142**, 417 (1985). Evidence for a periodicity of 400,000 years has been observed in Cretaceous shales [T. Herbert and A. Fischer, *Nature* **321**, 739 (1986)] and in deep-sea sediments in the Indian Ocean [ODP Leg 117 Shipboard Scientific Party, *ibid.* **331**, 663 (1988)].
26. Measurements of river water worldwide indicate that average modern runoff has a high $^{87}Sr/^{86}Sr$ ratio (R_r) of about 0.711 and provides a flux (J_r) of 3.0×10^{10} mol of Sr per year to the oceans; the average value of R_r from (*27*) is 0.7102, and the average R_r from M. Palmer and J. Edmond [*Earth Planet. Sci. Lett.* **92**, 11 (1989)] is 0.7119. We choose a value of 0.7110; if a different value were used it would change the details but not the main features of our models.
27. S. Goldstein and S. Jacobsen, *Chem. Geol.* **66**, 245 (1987).
28. Hydrothermal alteration and weathering of oceanic crust contributes Sr with a low $^{87}Sr/^{86}Sr$ ratio (0.7025 to 0.7055); see S. Hart, A. Erlank, F. Kable, *Contrib. Mineral. Petrol.* **44**, 219 (1974); E. Spooner, *Earth Planet. Sci. Lett.* **31**, 167 (1976); F. Albarède, A. Michard, J. Minster, G. Michard, *ibid.* **55**, 229 (1981). Because of the complexity of the exchange process, R_h is based on values for altered Samail ophiolite [McCulloch, R. Gregory, G. Wasserburg, H. Taylor, *Earth Planet. Sci. Lett.* **46**, 201 (1981)], fluids from Iceland [H. Elderfield and M. Greaves, *Geochim. Cosmochim. Acta* **45**, 2201 (1981)], and epidote from the Troodos ophiolite [B. Smith *et al.*, in *Symposium, Troodos '87: Ophiolites and Oceanic Lithosphere Abstr.* (Geological Survey Department, Nicosia, Cyprus, 1988) p. 162]. The modern $^{87}Sr/^{86}Sr$ ratio of the oceans and the better constrained values for the other fluxes are used to determine the product J_hR_h. A value of 0.705 for R_h corresponds to a J_h of 1.2×10^{10} mol per year. Current estimates of J_h range from 0.3×10^{10} to 1.4×10^{10} mol per year [see M. Delaney and E. Boyle, *Paleoceanography* **3**, 137 (1988)].
29. Dissolution and recrystallization of submarine carbonate sediments provides Sr with $^{87}Sr/^{86}Sr$ ratios mostly between 0.707 and 0.709. The ratio and flux for diagenesis of submarine sediments (R_c = 0.7085, $J_c = 3.0 \times 10^9$ mol per year) are based on studies of pore fluids [H. Elderfield and J. Gieskes, *Nature* **300**, 493 (1982); M. Palmer and H. Elderfield, *ibid.* **314**, 526 (1985)].
30. Based on a seawater Sr concentration of 7.65 ppm [see (*27*)].
31. We thank D. V. Kent, N. J. Shackleton, J. G. Moore, and the Deep Sea Drilling Project for providing samples. The manuscript was improved by comments from B. Stewart and two anonymous reviewers. An earlier version was reviewed by G. Bebout, F. Richter, and R. Shreve. This work was supported by donors of the Petroleum Research Fund, administered by the American Chemical Society, by National Science Foundation grants EAR 85-07995, EAR87-20609, and EAR88-04609 and by the director, Office of Energy Research, Office of Basic Energy Sciences, Engineering and Geosciences Division of the U.S. Department of Energy under contract No. DE-AC03-76SF00098.

1 February 1990; accepted 1 May 1990

Synchronous, Alternating, and Phase-Locked Stridulation by a Tropical Katydid

ENRICO SISMONDO

In the field the chirps of neighboring *Mecopoda* sp. (Orthoptera, Tettigoniidae, and Mecopodinae) males are normally synchronized, but between more distant individuals the chirps are either synchronous or regularly alternating. The phase response to single-stimulus chirps depends on both the phase and the intensity of the stimulus. Iteration of the Poincaré map of the phase response predicts a variety of phase-locked synchronization regimes, including period-doubling bifurcations, in close agreement with experimental observations. The versatile acoustic behavior of *Mecopoda* encompasses most of the phenomena found in other synchronizing insects and thus provides a general model of insect synchronization behavior.

INSECTS OF SEVERAL ORDERS PRODUCE rhythmic signals that are synchronous or regularly alternating with those of conspecific individuals. Notable examples are the songs of the cricket *Oecanthus* (*1*), the katydids *Pterophylla* (*2*), *Pholidoptera* (*3*), and *Ephippiger* (*4*), and the cicada *Magicicada* (*5*), as well as the flashing of the tropical fireflies *Pteroptyx* (*6, 7*). These phenomena have been explained in terms of inhibition-excitation (*3*), two proepisodic mechanisms (in which the stimulus precedes the chirp) (*1*), anticipatory versus paced synchronization (*6*), and the resetting of an internal pacemaker (*7*). I report an analysis of the song of *Mecopoda* species S (*8*): its acoustic behavior is analyzed in terms of the phase-response curve (PRC) and explored by iteration of the Poincaré map (*9*) and by numerical simulation of the interaction of two individuals.

The song of *Mecopoda* S consists of chirps (*10*) emitted every 1.5 to 3 s (Fig. 1, A and B): the chirp rate (CR) is temperature-dependent (Fig. 1C) in a manner consistent with that of other tettigoniids (*11*). In free run (without external stimulus), the period between the onset of successive chirps varies about the mean with a standard deviation in the range 35 to 45 ms (Fig. 1E) (*12*). The average CR in free run drifts with time (Fig. 1F). After entrainment to short-period stimuli, recovery to the free-run CR is slower than recovery time from long-period entrainment; to compensate for these effects, I used an empirical model to predict the "adapted" unconstrained period in simulation work (Fig. 1D). In the field, groups of males synchronize their chirps. Pairs separated by more than 3 to 4 m sometimes alternate chirps instead, each with a longer period than when synchronizing.

I generated artificial signals used for entrainment by computer-controlled playback of a digitized genuine chirp at controllable rate and intensity. Both stimulus and response chirps were recorded on separate tape channels; I then scanned the tape at 960 samples per second per channel to detect and record the onset of each chirp (*13*). Playback of a single isolated pulse from the stimulus chirp elicited normal response, with a minimum latency of 75 ± 9 ms; this length of time is much shorter than the duration of a complete chirp, justifying the use of stimulus onset as the analytical variable.

I obtained PRCs for 15 individuals,

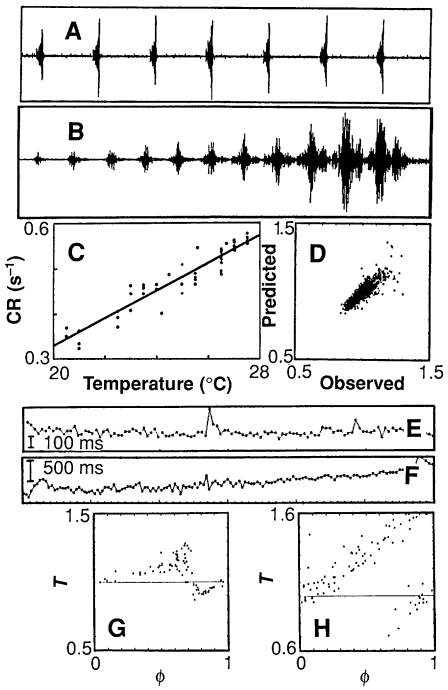

Fig. 1. (**A**) *Mecopoda* species S: A 12.6-s oscillogram of a series of chirps. (**B**) A 227-ms oscillogram of a typical single chirp. (**C**) Temperature dependence of CR (pooled data for three individuals and linear least-squares fit). (**D**) Empirical model of period adaptation function, predicted versus observed free period (normalized to T_0) after various entrainment episodes. (**E**) A 200-s free run showing cycle-to-cycle variation in chirp period. (**F**) A 240-s free run showing long-term drift in chirp period. (**G**) Atypical type I PRC (different individual from that shown in Fig. 2). (**H**) *Mecopoda* species N: PRC at 0 dB and 2.9 m.

22 Leedon Road, Singapore 1026, Republic of Singapore.